Final Technical Report

USGS Award Number:	G17AP00047
Title of Award:	Spatial correlation of ground motion characteristics for regional hazard and risk: regionalization and nonstationarity
Authors:	Jack Baker Stanford University Yang & Yamasaki Building, Room 283 423 Via Ortega Stanford, CA 94305-4020 650-725-2573 (telephone) 650-723-7514 (fax) bakerjw@stanford.edu Yilin Chen Stanford University 439 Panama Mall Building 02-540 Stanford CA 94305 yilinc2@stanford.edu
Term Covered by the Award:	7/1/2017 to 6/30/2018

Spatial Correlations of Response Spectra in New Zealand Strong Ground Motion Data

September 30, 2018

Abstract

This project utilized new techniques for quantifying spatial variations in strong ground motion, using ground motion data from recent well-recorded earthquakes in New Zealand. The data is unique in that many recording stations are relatively densely spaced, and that multiple strong earthquakes have been recorded at the same stations. The New Zealand ground motion network includes dense instrumentation (including strong ground motion stations spaced at 500 m in urban areas) in Wellington and Christchurch, and both of these regions have experienced repeated strong shaking in recent years. This enabled us to evaluate the typical hypotheses in spatial-correlation studies: that spatial variations are stationary in space and are not strongly location-specific or anisotropic in nature. We evaluated region-specific and site-specific spatial correlation models for Wellington and Christchurch, and studied how site-specific spatial correlation effects relate to physical phenomena that could be identified elsewhere in the world.

To date our studies have indicated some level of nonstationarity, but not at a level that clearly necessitates practical changes to current practice for quantifying spatial correlations. Our current hypothesis is that the first-order effect of nonstationarity is on mean ground shaking amplitudes, and that if these amplitude nonstationarities are accounted for by the ground motion model, the remaining correlations may not be strongly nonstationary. A related hypothesis is that if the nonstationarities are small in magnitude, they are difficult to precisely detect given the number of observations available at many of the considered sites. Our work will continue beyond the conclusion of this project, to continue quantifying nonstationarities, and evaluating the causes of nonstationarities (or lack thereof).

1 Introduction

This project aimed to develop new insights for quantifying spatial variations in strong ground motion, using newly available ground motion data from densely recorded earthquakes, where multiple strong earthquakes have been recorded at the same stations. The work enabled us to critically evaluate the typical hypotheses in spatial-correlation studies: that spatial variations are stationary in space and are not strongly location-specific or anisotropic in nature.

When an earthquake causes shaking in a region, the amplitude of shaking (measured, for example, using spectral acceleration at a given period) varies spatially. Some of that variation is predicable, via attenuation, near-surface site effects, basin effects, and other phenomena. Ground motion prediction models capture those effects, but there is significant remaining variation in ground motion amplitudes not captured by those models. This remaining variation in ground motion prediction "residuals" is significant, and shows spatial correlation at scales of tens of kilometers in separation distance. This spatial correlation is expected, due to commonalities in crustal velocity structure and wave propagation paths, and has been shown by a number of researchers to be important when assessing risk to spatially distributed infrastructure or portfolios of properties.

The present typical assumption in regional ground motion modeling to assume that these ground motion amplitude spatial correlations are constant around the world (at least for crustal earthquakes). That is, we assume that the correlation in shaking amplitude at two sites separated by 10 km is the same, whether the two sites are located in California or Japan or New Zealand. Further, we assume that the spatial correlation of shaking amplitude at two sites in a given region is the the same whether the sites have similar or differing geologic conditions. These assumptions of *stationarity* in spatial correlations have been made out of necessity, as earthquakes are rare, and dense networks of strong ground motion instruments are sparse, so that we typically cannot obtain the data needed to refine these assumptions.

Quantifying variation in ground-motion amplitude over a spatially-distributed region is of interest for studies of spatially distributed systems. Quantification typically consists of measuring correlation between the ground-motion intensities at different sites during a single event. Studies of these spatial correlations have been performed in the past by a number of researchers (e.g., Boore et al. 2003; Wang and Takada 2005; Goda and Hong 2008; Baker and Jayaram 2008; Jayaram and Baker 2009a; Foulser-Piggott and Stafford 2011; Goda and Atkinson 2010; Goda 2011; Loth and Baker 2013). These studies produce predictive equations for the correlation coefficient as a function of the period of interest

and the separation distance between two considered sites.

2 Data

In this study, we used New Zealand strong ground motion data from Van Houtte et al. (2017). We consider all recordings with closest distance to the fault rupture (R_{rup}) less than 100 km and magnitude greater than 3. Although this filtering keeps some small-magnitude subduction zone events that are out of the suggested magnitude range by the ground motion model ($M_w > 5$), it is neccessary in order to retain a sufficient number of repeated ground motions at many stations, so that we can estimate site-specific correlations. We assume that that this decision has not had a substantial impact on estimated correlations, but further work is planned to evaluate this issue in more detail.

Table 1 shows a selection of well-recorded earthquakes in the database. There are a substantial number of earthquakes with dozens of strong-motion recordings, allowing for characterization of correlations in ground motion amplitudes between recording stations.

The New Zealand cities of Christchurch and Wellington are of particular interest for this study, as they contain the most dense instrumentation in the country, and have repeated observations of strong shaking. Table 3 and 2 list the stations in these two regions with at least seven recordings meeting the above selection criteria.

Table 1: Selection of earthquakes from Van Houtte et al. (2017).

CuspID	M_w	**Tectonic Class**	**Region**	**Number of recordings**
2016p858000	7.85	Crustal	Wellington	88
2016p118944	5.76	Crustal	Christchurch	52
2013p543824	6.58	Crustal	Wellington	48
2013p613797	6.6	Crustal	Wellington	48
3631380	5.85	Crustal	Christchurch	46
3631359	5.79	Crustal	Christchurch	45
2354133	5.31	Slab	Wellington	44
2013p542711	5.74	Crustal	Wellington	43
3366146	7.08	Crustal	Christchurch	41
2625245	4.57	Slab	Wellington	41
2567873	4.54	Slab	Wellington	40
3528839	5.99	Crustal	Christchurch	39
3765940	3.79	Crustal	Wellington	38
2013p614135	5.9	Crustal	Wellington	37
3734186	4.66	Crustal	Christchurch	37
3711648	5.07	Crustal	Christchurch	37
2499328	4.24	Slab	Wellington	37
3528810	5.3	Crustal	Christchurch	36
2352986	5.18	Interface	Wellington	36
2013p563639	4.86	Crustal	Wellington	36
3413873	5.0	Slab	Wellington	35
2359081	5.1	Interface	Wellington	34
2654849	4.72	Slab	Wellington	32

Table 2: Utilized recording stations in the Christchurch region.

SiteCode	Latitude	Longitude	Region	Number of recordings
CMHS	-43.5656	172.6242	Christchurch	19
CACS	-43.4832	172.5300	Christchurch	18
CBGS	-43.5293	172.6199	Christchurch	18
DSLC	-43.6675	172.1979	Christchurch	17
PPHS	-43.4928	172.6069	Christchurch	17
REHS	-43.5219	172.6351	Christchurch	14
ASHS	-43.2744	172.5959	Christchurch	13
NNBS	-43.4954	172.7180	Christchurch	13
DHSS	-43.6303	172.7272	Christchurch	12
HHSS	-43.5575	172.5928	Christchurch	12
RHSC	-43.5362	172.5644	Christchurch	12
STKS	-43.6065	172.6449	Christchurch	12
SUMS	-43.5692	172.7568	Christchurch	12
TPLC	-43.5500	172.4720	Christchurch	12
HUNS	-43.5794	172.6572	Christchurch	11
KPOC	-43.3765	172.6638	Christchurch	11
LINC	-43.6232	172.4680	Christchurch	11
MTPS	-43.5847	172.7256	Christchurch	11
SLRC	-43.6751	172.3175	Christchurch	11
SWNC	-43.3694	172.4954	Christchurch	11
CSTC	-43.3123	172.3813	Christchurch	10
GODS	-43.5783	172.7704	Christchurch	10
HVSC	-43.5798	172.7094	Christchurch	10
LPCC	-43.6078	172.7248	Christchurch	10
MORS	-43.5395	172.6214	Christchurch	10
MPSS	-43.4994	172.6423	Christchurch	10
NBLC	-43.5069	172.7314	Christchurch	10
OHSS	-43.4446	172.6605	Christchurch	10
PARS	-43.5679	172.7507	Christchurch	10
SHLC	-43.5053	172.6634	Christchurch	10
D14C	-43.6325	172.6247	Christchurch	9
MENS	-43.5585	172.7115	Christchurch	9
SMTC	-43.4675	172.6139	Christchurch	9
CHHC	-43.5359	172.6275	Christchurch	8
OPWS	-43.5562	172.6643	Christchurch	8

CCCC	-43.5381	172.6474	Christchurch	7
CRLZ	-43.5747	172.6232	Christchurch	7
EYRS	-43.4214	172.3554	Christchurch	7
HALS	-43.5909	172.5695	Christchurch	7
MQZ	-43.7061	172.6538	Christchurch	7
PRPC	-43.5258	172.6828	Christchurch	7

Table 3: Utilized recording stations in the Wellington region.

SiteCode	Latitude	Longitude	Region	Number of recordings
WNKS	-41.2848	174.7421	Wellington	22
ARKS	-41.2421	174.9441	Wellington	21
LHES	-41.2117	174.9033	Wellington	21
TFSS	-41.2754	174.7831	Wellington	21
WNAS	-41.3264	174.8090	Wellington	20
MISS	-41.3149	174.8184	Wellington	19
PGMS	-41.2245	174.8794	Wellington	19
POLS	-41.1314	174.8391	Wellington	19
WEL	-41.2840	174.7682	Wellington	19
WEMS	-41.2743	174.7793	Wellington	19
WNHS	-41.3008	174.7755	Wellington	19
FKPS	-41.2879	174.7788	Wellington	18
LHRS	-41.2047	174.8932	Wellington	18
EBPS	-41.2894	174.9002	Wellington	17
POTS	-41.2722	174.7746	Wellington	17
UHCS	-41.1268	175.0409	Wellington	17
FAIS	-41.2074	174.9401	Wellington	16
LHBS	-41.1966	174.8923	Wellington	15
PFAS	-41.1385	174.8461	Wellington	15
RQGS	-41.2965	174.7812	Wellington	15
TEPS	-41.2906	174.7811	Wellington	15
WDAS	-41.2574	174.9485	Wellington	15
INSS	-41.2335	174.9211	Wellington	14
MKBS	-41.2259	174.6981	Wellington	14
LHUS	-41.2308	174.8936	Wellington	13
NEWS	-41.2320	174.8218	Wellington	13
BMTS	-41.1914	174.9260	Wellington	12
SOCS	-41.2043	174.9159	Wellington	12
468A	-41.2011	174.9547	Wellington	11
HSSS	-41.1519	174.9815	Wellington	11
PWES	-41.1275	174.8259	Wellington	11
SNZO	-41.3087	174.7042	Wellington	11
NBSS	-41.2023	174.9538	Wellington	10
WANS	-41.2312	174.9310	Wellington	10
467A	-41.2425	174.9024	Wellington	9

DAVS	-41.2058	174.9544	Wellington	9
PHFS	-41.2526	174.9045	Wellington	9
SOMS	-41.2575	174.8650	Wellington	9
TMDS	-41.0781	175.1554	Wellington	9
464A	-41.2308	174.9135	Wellington	8
VUWS	-41.2799	174.7784	Wellington	8
PHHS	-41.2521	174.9043	Wellington	7
PVCS	-41.2247	174.8739	Wellington	7
SEAS	-41.3264	174.8376	Wellington	7
TOTS	-41.1049	175.0854	Wellington	7
TRTS	-41.2987	174.7739	Wellington	7

3 Methodology

This section describes the calculations utilized to compute ground motion residuals and spatial correlations.

3.1 Within-event residuals

Consider a typical ground motion model for spectral accelerations

$$\ln SA_{i,j} = \mu_{\ln SA}(Rup_{i,j}, Site_j) + \delta B_i + \delta W_{i,j} \tag{1}$$

where $SA_{i,j}$ is the spectral acceleration at the period of interest at site j caused by i^{th} rupture; $\mu_{\ln SA}(Rup_{i,j}, Site_j)$ is the predicted natural logarithmic mean of spectral acceleration intensity; δB_i is the between-event residual for the i^{th} rupture; $\delta W_{i,j}$ is the within-event residual for site j from the i^{th} rupture. The ground motion model specifies $\mu_{\ln SA}(Rup_{i,j}, Site_j)$, as well as the standard deviations of δB_i and $\delta W_{i,j}$, denoted τ and ϕ, respectively.

In this study, the Abrahamson et al. (2016) ground motion model is used for subduction zone events, and the Chiou and Youngs (2014) model is used for crustal events. Figure 1 shows an example of two ground motion predictions.

For each earthquake and station considered in this study, we have an observed $\ln SA_{i,j}$, and predicted $\mu_{\ln SA}(Rup_{i,j}, Site_j)$, τ and ϕ from the ground motion model. Subtracting the observation from the predicted mean gives a total residual (illustrated in Figure 1), and then the mixed effects regression approach described by Stafford (2012) is used to estimate δB_i for each earthquake and $\delta W_{i,j}$ for each ground motion.

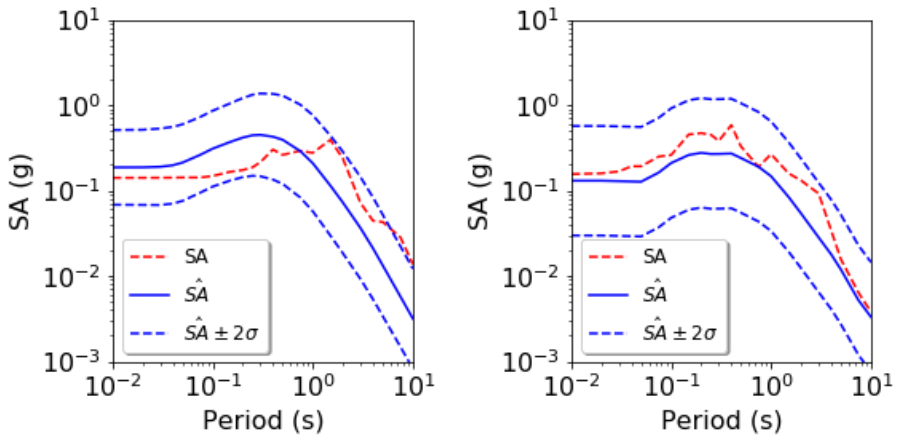

(a) (b)

Figure 1: Example observed ground motion response spectra and ground motion predictions as used in this study. $\hat{SA}$ denotes the exponential of $\mu_{\ln SA}(Rup_{i,j}, Site_j)$, and $\hat{SA} \pm \sigma$ denotes $\pm$ two standard deviation intervals on $\mu_{\ln SA}(Rup_{i,j}, Site_j)$ predicted by the ground motion model. (a) Station TAFS recording of the M_w 7.2 Fiordland earthquake (R_{rup} = 46.6km), and the prediction from Abrahamson et al. (2016). (b) Station WEMS recording of the M_w 7.8 Kaikoura earthquake (R_{rup} = 49.7km), and the prediction from Chiou and Youngs (2014).

3.2 Correlation coefficients

For every pair of stations (j, k), we select all earthquakes with suitable recordings at both stations, and use equation 2 to calculate the correlation coefficient in within-event residuals

$$\hat{\rho}(j,k) = \frac{\sum_{i=1}^{n}(\delta W_{i,j} - \delta\bar{W}_{i,j})(\delta W_{i,k} - \delta\bar{W}_{i,k})}{\sqrt{\sum_{i=1}^{n}(\delta W_{i,j} - \delta\bar{W}_{i,j})^2}\sqrt{\sum_{i=1}^{n}(\delta W_{i,k} - \delta\bar{W}_{i,k})^2}} \tag{2}$$

where n is the number of earthquakes with pairs of recordings at the given stations.

Through some experimentation, we determined that stable estimates of correlation coefficients were best obtained by considering only pairs of stations with at least seven pairs of within-event residuals. Bowley (1928) shows that the standard deviation of the correlation coefficient of sample size n is given by:

$$std(\hat{\rho}) = \sqrt{\frac{1-\rho^2}{n}} \tag{3}$$

Figure 2 shows the standard deviation of the sample correlation coefficient, as a function of the true correlation and the number of observation pairs.

Figure 3 shows an example of the correlation coefficient of within-event residuals at station WEMS and POTS. Table 4 shows the information of common earthquakes used at station WEMS and POTS.

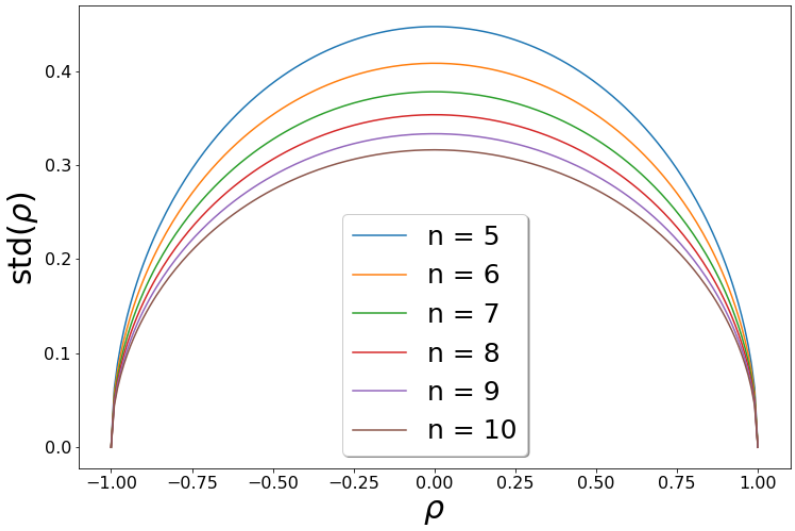

Figure 2: Standard deviation of sample correlation coefficient (ρ) as a function of sample size (n) and true correlation coefficient (ρ).

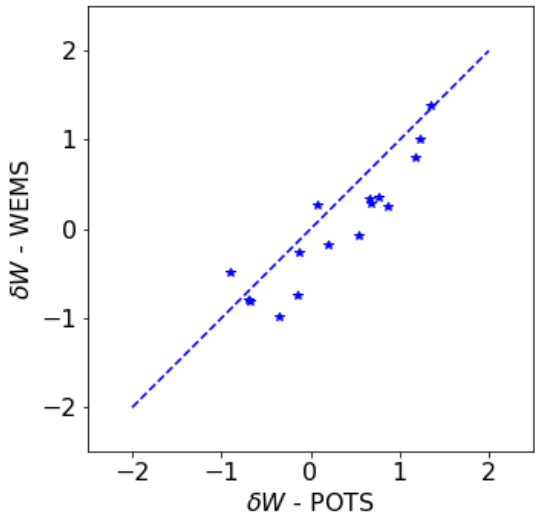

Figure 3: Scatter plot of within-event residuals of one-second spectral acceleration at POTS and WEMS ($d = 0.46$ km.). A line with a slope of 1 is included for reference. The estimated correlation coefficient for these data is $\hat{\rho} = 0.91$.

Table 4: Earthquakes with suitable recordings at stations WEMS and POTS.

CuspID	M_w	**Tectonic Class**	$\delta_{W,WEMS}$	$\delta_{W,POTS}$
2625245	4.57	Slab	0.29	0.68
2499328	4.24	Slab	-0.74	-0.15
2016p858000	7.85	Crustal	0.80	1.17
3413873	5.00	Slab	-0.80	-0.69
3765940	3.79	Crustal	0.25	0.86
2013p613947	5.18	Crustal	0.36	0.76
2013p613797	6.60	Crustal	1.00	1.23
2013p563639	4.86	Crustal	0.34	0.66
2567873	4.54	Slab	-0.07	0.54
3145159	4.70	Slab	-0.81	-0.68
2013p543824	6.58	Crustal	1.39	1.34
2013p542711	5.74	Crustal	0.28	0.08
2692934	4.20	Slab	-0.99	-0.35
1502698	5.25	Slab	-0.18	0.19
2354133	5.31	Slab	-0.49	-0.90
2352986	5.18	Interface	-0.26	-0.12

3.3 Deviation of correlation coefficients from a stationary model

After calculating the correlation coefficients of all pairs of stations in the database, we can evaluate site-specific deviation of these correlations relative to a reference model. Jayaram and Baker (2008) showed that spatially distributed pair of within-event residuals can be represented by a bivariate normal distribution. Under this assumption, Fisher's z-transformation can be applied to identify correlation deviation. The Fisher's z-transformation is

$$z_{\hat{\rho}} = \frac{1}{2} ln(\frac{1+\hat{\rho}}{1-\hat{\rho}}) \tag{4}$$

where $\hat{\rho}$ is the sample correlation coefficient. For a sample of observations, $z_{\hat{\rho}}$ is approximately normally distributed with mean $\frac{1}{2} ln(\frac{1+\rho}{1-\rho})$ and standard deviation $\frac{1}{\sqrt{n-3}}$, where ρ is the true correlation coefficient and n is the number of paired observations.

Then we can define

$$e = (z_{\hat{\rho}} - z_{\rho}) \times \sqrt{n-3} \tag{5}$$

as the measure of correlation deviation. Under the above assumptions, e will follow the standard normal distribution.

4 Results

This section presents results to date using the above approaches. All results use the data described above, and are presented for five-percent-damped spectral acceleration at a period of 1 second ($SA(1s)$). This spectral acceleration period was chosen as it is potentially sensitive to effects of deep geologic structure such as sedimentary basins, but is not such a long period that recording stations have difficulty reliably measuring it.

4.1 Stationary and isotropic spatial correlation

In order to evaluate the Pearson's correlation coefficient results under stationarity and isotropy assumptions, we average the correlation coefficients of all pairs of sites separated by the same distance:

$$\bar{\rho}(h) = \frac{1}{N} \sum_{|d(\boldsymbol{j},\boldsymbol{k})-h|<b} \hat{\rho}(\boldsymbol{j},\boldsymbol{k}) \tag{6}$$

where the summation condition takes the average of the correlation coefficients of all pairs of sites with distance from $h - b$ to $h + b$. In this case, the non-stationary and anisotropic effects are averaged out. A model developed by Jayaram and Baker (2009b) is used as the reference model here.

Figure 4 shows data from this study using the above approach. It can be seen that the average correlation decreases with separation distance, as expected, although there is significant variation relative to the average at individual station pairs. The average correlation also corresponds well to the reference Jayaram and Baker (2009b) model. This suggests that the data set under consideration is consistent with data used in prior empirical spatial correlation studies such as Jayaram and Baker (2009b).

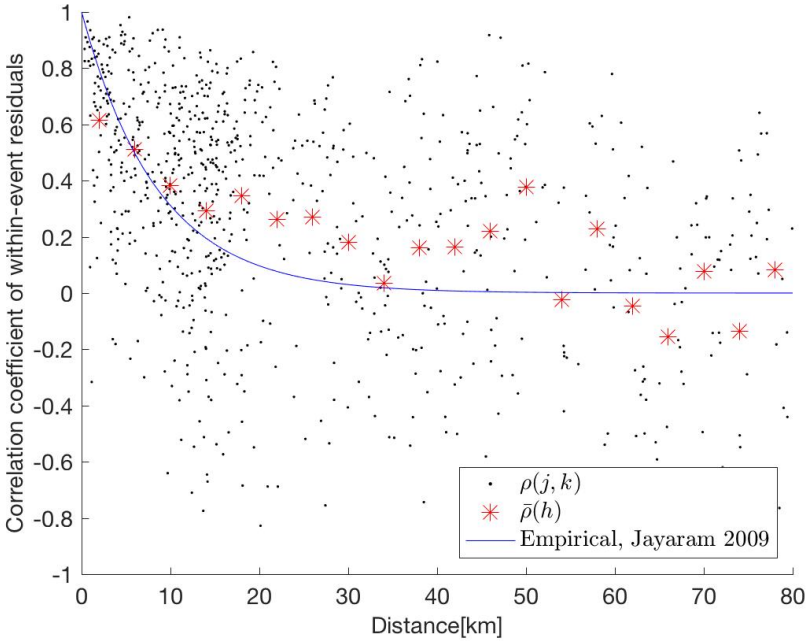

Figure 4: Correlation coefficients for $SA(1s)$ within-event residuals as a function of station separation distance.

4.2 Non-stationary spatial correlation

We next use equation 5 to measure the deviations of individual correlations from the (Jayaram and Baker 2009b) reference model. Figure 5 shows the highlights the station pairs that are most deviated from the reference model given separation distance less than 10 km.

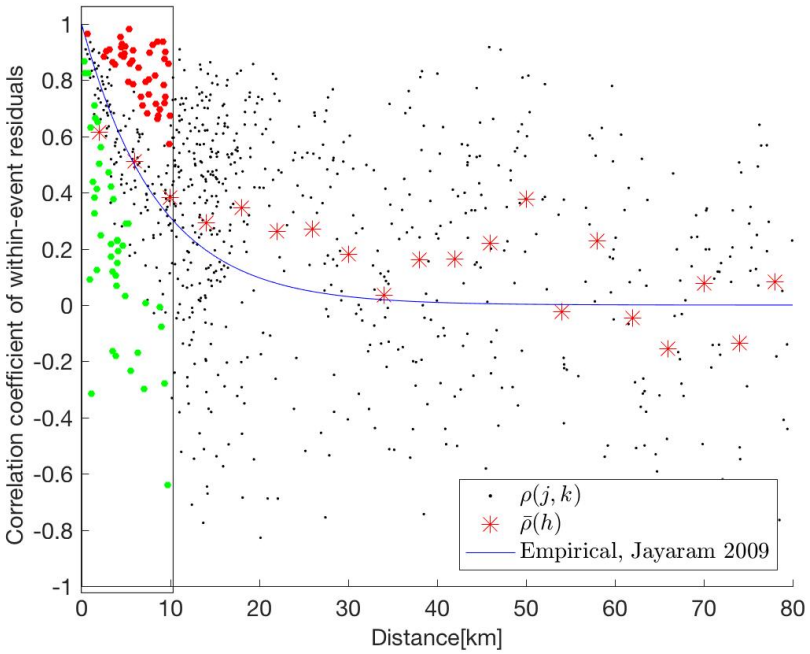

Figure 5: Correlation coefficients for $SA(1s)$ within-event residuals as a function of station separation distance. Red dots show the correlations for the 20% of station pairs with the largest correlation coefficients relative to model predictions, and green dots show correlations for the smallest 20%.

Figure 6 shows the location of high- and low-correlated pairs of stations in the Wellington region. Red and green lines are used to connect station pairs with high and low correlations, respectively. The southwest portion of the map (near downtown Wellington) seems to have systematically lower correlations than the stationary reference model, while the northeast region has systematically higher correlations. This may be because many of the low-correlation pairs in the southeast have a station at the edge of the sedimentary basin and a station on rock, while the station pairs in the northeast are on more homogeneous site conditions (Bradley et al. 2017). If true, this would indicate that changes in geologic condition cause greater variation in ground shaking for a given separation distance, and tend to lower correlations in ground shaking intensity. While the hypothesis is intuitively reasonable, we believe that this is the first empirical observation of such an effect in strong motion data, and points towards a path for incorporating such effects in a predictive model.

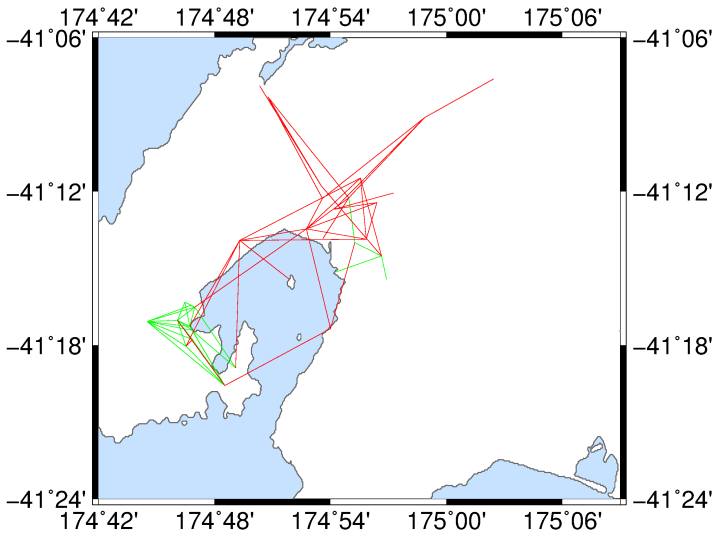

Figure 6: Locations of station pairs in Wellington with high or low correlations relative to the reference correlation model. Pairs with the highest 20% of correlation deviations are connected with red lines and pairs with the lowest 20% of correlation deviations are connected with green lines.

Figure 7 shows the location of high- and low-correlated pairs of stations in the Christchurch region. We did not observe any regions where there appear to be systematically higher or lower correlations than the stationary model predicts. This may be because the site conditions for the station pairs shown here are generally similar, relative to the variations that were seen in the Wellington station pairs.

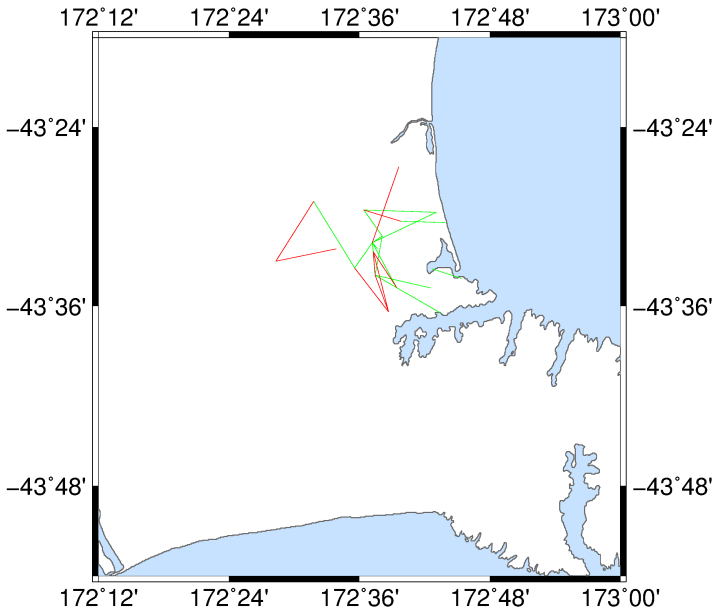

Figure 7: Locations of station pairs in Christchurch with high or low correlations relative to the reference correlation model. Pairs with the highest 20% of correlation deviations are connected with red lines and pairs with the lowest 20% of correlation deviations are connected with green lines.

4.3 Magnitude dependence of spatial correlations

We quantify the influence of a earthquake on correlation by comparing the sample correlation coefficients with and without the earthquake. Specifically, the influence of earthquake i on the correlation at a pair of station is defined as

$$h = (z_{\hat{\rho}_{-i}} - z_{\hat{\rho}}) \times \sqrt{n-3} \tag{7}$$

where $z_{\hat{\rho}}$ is the Fisher-z-transformed correlation estimate as defined above, and $z_{\hat{\rho}_{-i}}$ is the the same transformed correlation, but with the correlation coefficient estimated after omitting data from earthquake i. A negative h score means that earthquake i increases the correlation at a given pair of stations (because its omission decreases the correlation), and vice versa. Figure 8 shows the h scores of all earthquakes and all pairs of stations.

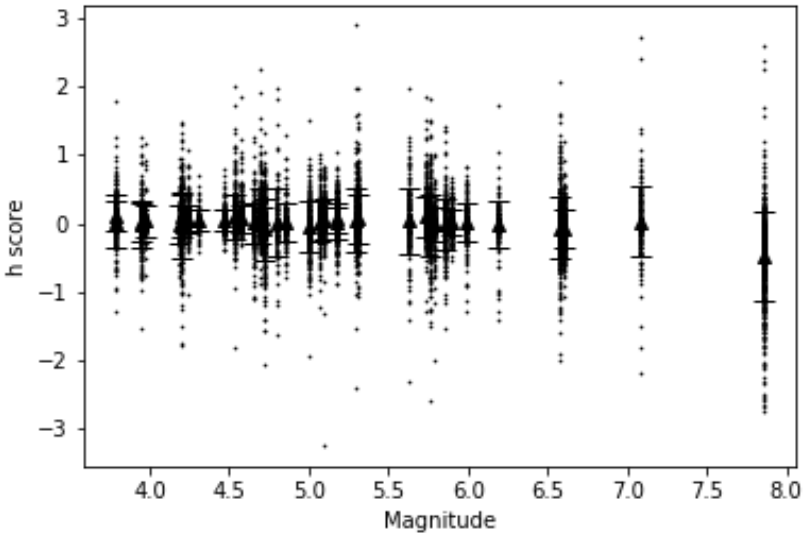

Figure 8: Computed h score from Equation 7 for all earthquakes and station pairs, plotted versus earthquake magnitude. Triangles indicate the mean of the h scores and bars show the $\pm$ standard deviations.

The mean h scores for most earthquakes are around zero, which indicates that the correlation caused by these earthquakes are consistent with each other. However, the M_w 7.8 Kaikoura earthquake has a mean of -0.4 and higher standard deviation, and it also possesses some extreme h scores. It is speculated the M_w 7.8 Kaikoura earthquake has large within-event residuals, and thus adding or removing the earthquake data will influence the correlation coefficient substantially.

Figure 9 shows the histograms of h scores of M_w 7.1 Darfield and M_w 7.8 Kaikoura earthquake. The distribution of h score of these two earthquakes are quite different. The M_w 7.8 Kaikoura event causes higher correlations (i.e., it has a negative mean), while the Darfield earthquake is consistent with the overall correlation level, and the Darfield has lighter distribution tails. It is speculated that the ground motion model did not predict well for the M_w 7.8 Kaikoura earthquake, since this earthquake involved complex rupture of a number of faults (Bradley et al. 2018) and the general rupture parameters such as R_{rup} are too simple to compute resulting ground motion, which causes regional deviation of predictions and thus results in high correlations of prediction residuals. On the other hand, the M_w 7.1 Darfield earthquake had a somewhat simpler rupture, and ground motion amplitudes are more easily predicted as a function of R_{rup},

leading to fewer regional deviations in ground motion amplitudes and thus no systematic correlation effects. If true more generally, this pattern may suggest a relationship between rupture complexity and spatial correlations in ground motion residuals.

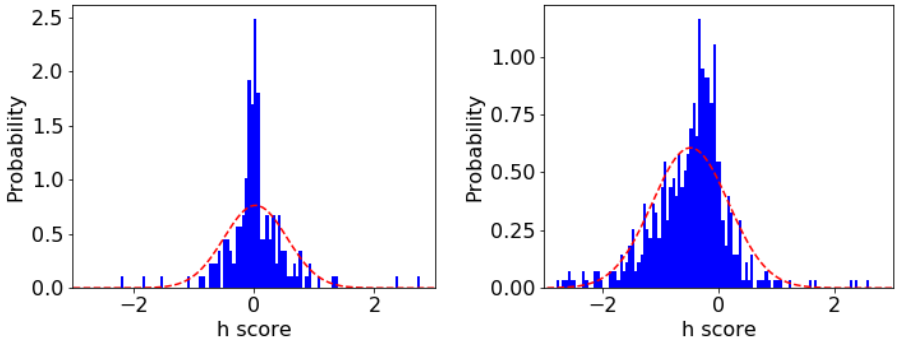

(a) (b)

Figure 9: Histogram of h scores of the M_w 7.1 Darfield (a) and M_w 7.8 Kaikoura (b) earthquakes. Red lines show the probability density function of the normal distribution estimated from the histogram.

Figures 12 and 10 show the within-event residuals for the Darfield and Kaikoura earthquakes. For the Kaikoura earthquake (Figure 10), the regional clustering of within-event residuals is noticeable. For example, negative within-event residuals cluster in the Wellington region and positive within-event residuals cluster in the Christchurch region (highlighted in more detail in Figure 11). Therefore, recordings from this event tend to imply high spatial correlations, and thus can result in low h scores, as observed above. As for the Darfield earthquake (Figure 12), there is no apparent regional clustering of residuals. Therefore, removing this event from the correlation coefficient calculation has less influence on estimated spatial correlations, resulting in the h scores that are close to zero on average, and with few extreme values.

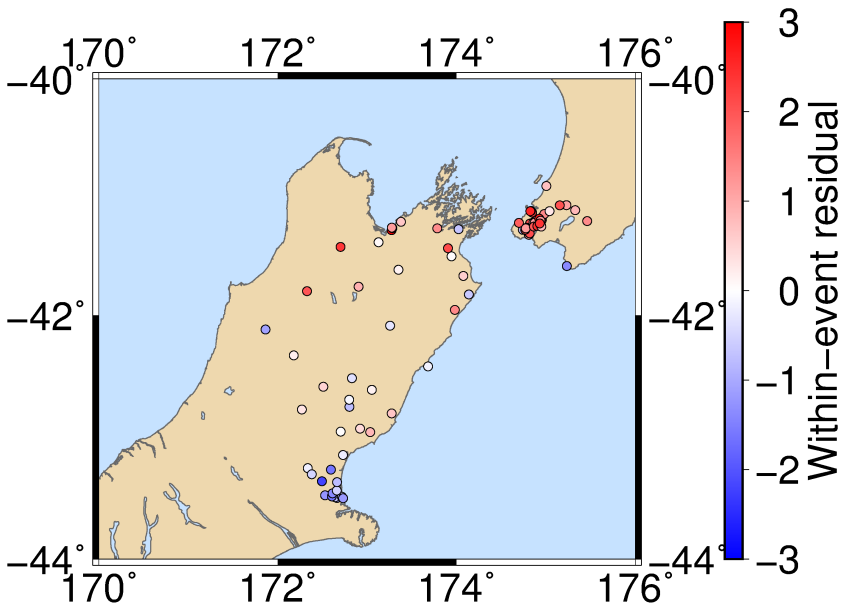

Figure 10: $SA(1s)$ within-event residuals from the M_w 7.8 Kaikoura earthquake.

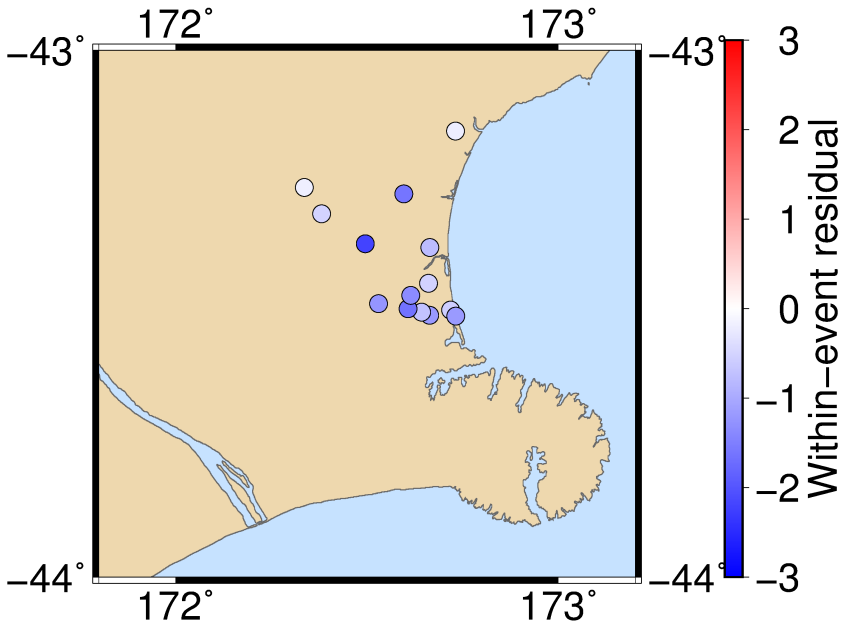

(a)

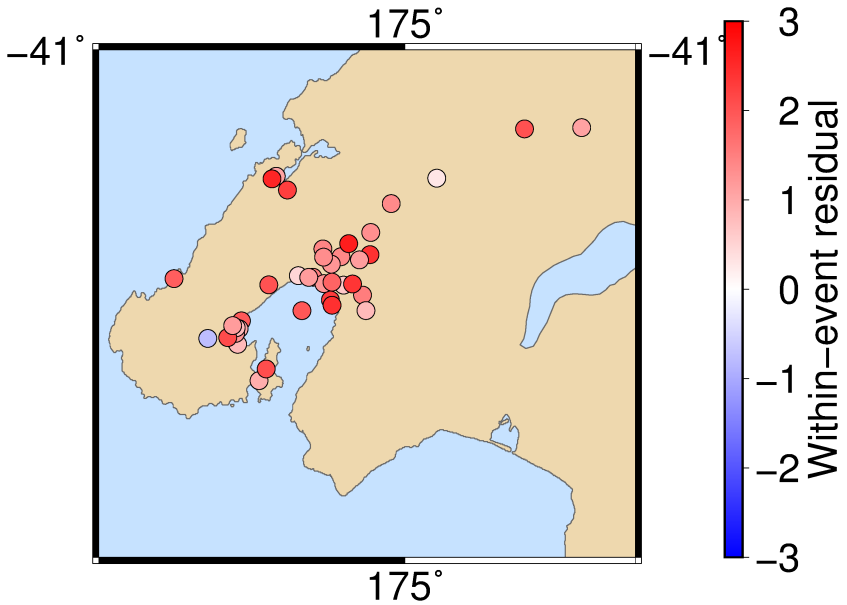

(b)

Figure 11: One-second spectral acceleration within-event residuals from the M_w 7.8 Kaikoura earthquake at Christchurch (a) and Wellington (b).

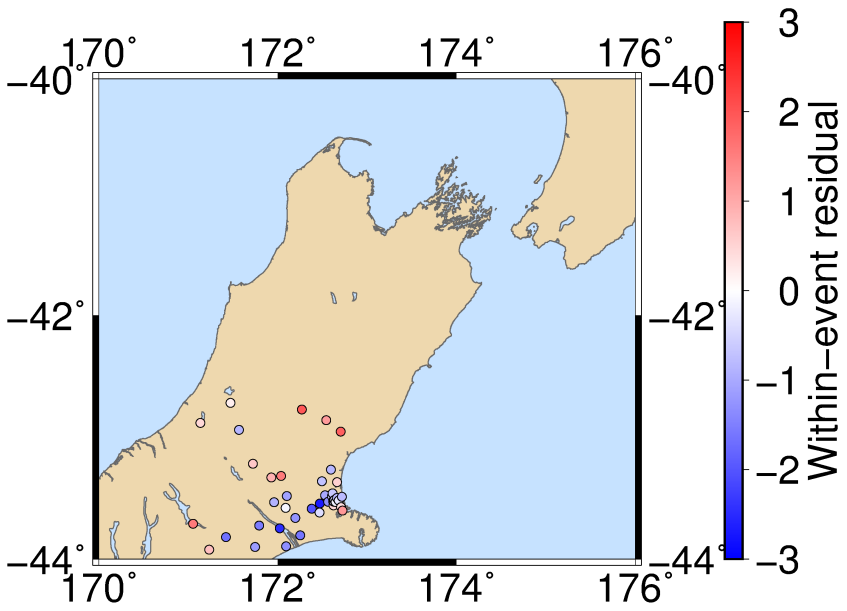

Figure 12: $SA(1s)$ within-event residuals from the M_w 7.1 Darfield earthquake.

5 Conclusions

This report documents the most promising of the spatial correlation assessment approaches explored over the course of this project, and presents numerical results from New Zealand strong ground motion data. On average, the New Zealand ground motions have spatial correlations comparable to a reference model that was previously calibrated based on global data sets. Looking at spatial correlations from particular events or station pairs, the results indicated some level of nonstationarity in correlations.

Potential sources of nonstationarity are geologic conditions and rupture complexity. For geologic conditions, heterogeneous conditions in Wellington appear to be associated with lower spatial correlations than under more homogeneous conditions. This is consistent with intuition that site-condition changes may cause amplitude variations to a degree that is not captured by the ground motion model, leading to a reduction in correlation of residuals. For rupture complexity, the extremely complex Kaikoura rupture produced larger spatial correlations than other events in the database. This may be because the com-

plexity is not captured by the ground motion model's simple parameterization of the rupture via magnitude and closest distance to the rupture, leading to regional variations in ground shaking amplitude that are not explained by the mean ground motion model prediction, and thus persist as (spatially correlated) within-event residuals.

The robustness of these observations in other conditions, and the impact of these nonstationarities on regional risk assessments, is not yet clear. Our work will continue beyond the conclusion of this project, to continue quantifying nonstationarities, and evaluating the causes of nonstationarities (or lack thereof).

6 Acknowledgements

We thank Brendon Bradley for help in interpreting these data and providing feedback on ground motion predictions, and Chris Van Houtte for clarifications regarding the ground motion database.

References

Abrahamson, Norman, Nicholas Gregor, and Kofi Addo (2016). "BC Hydro ground motion prediction equations for subduction earthquakes". In: *Earthquake Spectra* 32.1, pp. 23–44.

Baker, Jack W. and Nirmal Jayaram (2008). "Correlation of spectral acceleration values from NGA ground motion models". In: *Earthquake Spectra* 24.1, pp. 299–317. DOI: 10.1193/1.2857544.

Boore, David M. et al. (2003). "Estimated Ground Motion From the 1994 Northridge, California, Earthquake at the Site of the Interstate 10 and La Cienega Boulevard Bridge Collapse, West Los Angeles, California". In: *Bulletin of the Seismological Society of America* 93.6, pp. 2737–2751.

Bowley, AL (1928). "The standard deviation of the correlation coefficient". In: *Journal of the American Statistical Association* 23.161, pp. 31–34.

Bradley, Brendon A, Liam M Wotherspoon, and Anna E Kaiser (2017). "Ground motion and site effect observations in the Wellington region from the 2016 Mw 7.8 Kaikura, New Zealand, earthquake". In: *Bull. New Zeal. Soc. Earthq. Eng.* 2, pp. 94–105.

Bradley, Brendon A et al. (2018). "Influence of site effects on observed ground motions in the Wellington region from the M w 7.8 Kaikura, New Zealand, earthquake". In: *Bulletin of the Seismological Society of America*.

Chiou, Brian S-J and Robert R Youngs (2014). "Update of the Chiou and Youngs NGA model for the average horizontal component of peak ground motion and response spectra". In: *Earthquake Spectra* 30.3, pp. 1117–1153.

Foulser-Piggott, Roxane and Peter J. Stafford (2011). "A predictive model for Arias intensity at multiple sites and consideration of spatial correlations". In: *Earthquake Engineering & Structural Dynamics*, n/a.

Goda, Katsuichiro (2011). "Interevent Variability of Spatial Correlation of Peak Ground Motions and Response Spectra". In: *Bulletin of the Seismological Society of America* 101.5, pp. 2522–2531. DOI: 10.1785/0120110092.

Goda, Katsuichiro and Gail M. Atkinson (2010). "Intraevent Spatial Correlation of Ground-Motion Parameters Using SK-net Data". In: *Bulletin of the Seismological Society of America* 100.6, pp. 3055–3067. DOI: 10.1785/0120100031.

Goda, Katsuichiro and H. P. Hong (2008). "Spatial Correlation of Peak Ground Motions and Response Spectra". In: *Bulletin of the Seismological Society of America* 98.1, pp. 354–365. DOI: 10.1785/0120070078.

Jayaram, Nirmal and Jack W Baker (2008). "Statistical tests of the joint distribution of spectral acceleration values". In: *Bulletin of the Seismological Society of America* 98.5, pp. 2231–2243.

Jayaram, Nirmal and Jack W. Baker (2009a). "Correlation model for spatially distributed ground-motion intensities". In: *Earthquake Engineering & Structural Dynamics* 38.15, pp. 1687–1708. DOI: 10.1002/eqe.922.

Jayaram, Nirmal and Jack W Baker (2009b). "Correlation model for spatially distributed ground-motion intensities". In: *Earthquake Engineering & Structural Dynamics* 38.15, pp. 1687–1708.

Loth, Christophe and Jack W. Baker (2013). "A spatial cross-correlation model for ground motion spectral accelerations at multiple periods". In: *Earthquake Engineering & Structural Dynamics* 42.3, pp. 397–417. DOI: DOI:10.1002/eqe.2212.

Stafford, Peter J (2012). "Evaluation of structural performance in the immediate aftermath of an earthquake: a case study of the 2011 Christchurch earthquake". In: *International Journal of Forensic Engineering* 1.1, pp. 58–77.

Van Houtte, Chris et al. (2017). "The New Zealand strong motion database". In: *Bull. New Zeal. Soc. Earthq. Eng.* 50.1.

Wang, Min and Tsuyoshi Takada (2005). "Macrospatial Correlation Model of Seismic Ground Motions". In: *Earthquake Spectra* 21.4, pp. 1137–1156.